

The Modified Ghost Fluid Method Applied to Fluid-Elastic Structure Interaction

Tiegang Liu¹, A. W. Chowdhury² and Boo Cheong Khoo^{2,3,*}

¹ LMIB and School of Mathematics and Systems Science, Beijing University of Aeronautics and Astronautics, Beijing 100191, China

² Department of Mechanical Engineering, National University of Singapore, Singapore 119260, Singapore

³ Singapore-MIT Alliance, 4 Engineering Drive 3, National University of Singapore, Singapore 117576, Singapore

Received 13 September 2010; Accepted (in revised version) 24 February 2011

Available online 9 September 2011

Abstract. In this work, the modified ghost fluid method is developed to deal with 2D compressible fluid interacting with elastic solid in an Euler-Lagrange coupled system. In applying the modified Ghost Fluid Method to treat the fluid-elastic solid coupling, the Navier equations for elastic solid are cast into a system similar to the Euler equations but in Lagrangian coordinates. Furthermore, to take into account the influence of material deformation and nonlinear wave interaction at the interface, an Euler-Lagrange Riemann problem is constructed and solved approximately along the normal direction of the interface to predict the interfacial status and then define the ghost fluid and ghost solid states. Numerical tests are presented to verify the resultant method.

AMS subject classifications: 65M06, 65N85, 74F10, 35L65, 35L67, 35Q74

Key words: Fluid-elastic structure interaction, Euler-Lagrange coupling, Euler-Lagrange Riemann problem, ghost fluid method, modified ghost fluid method.

1 Introduction

Fluid-structure interaction (FSI) is one important field of scientific interests [17]; it covers numerous applications including acoustics, explosive loading of structures, fluid induced vibration of floating/offshore structures, sloshing of liquids in open and closed containers, wind load on buildings, flutter of aerodynamic vehicles, etc. In this work, our focus is on the numerical treatment of compressible fluid-elastic structure interaction.

*Corresponding author.

URL: <http://serve.me.nus.edu.sg/khoobc/>

Email: liutg@buaa.edu.cn (T. G. Liu), mpekbc@nus.edu.sg (B. C. Khoo)

There are several difficulties and challenges encountered in the numerical simulation of FSI. The first issue is how to treat the coupling between the fluid domain and solid domain. The second is numerical instability, especially when the structure is under a strong impact. The third is to faithfully take into account the nonlinear interaction occurring at the interface.

In treatment of the first issue [18, 19], there are several ways as founded in the literature and these can generally be categorized as three approaches, namely, the loose Euler-Lagrange coupling, full Lagrange coupling and half-way Euler-Lagrange coupling. The loose Euler-Lagrange coupling is a weak coupling and very popular, where the fluid domain and the solid domain are solved by a fluid solver (usually an Eulerian solver such as a finite difference method) and a solid solver (usually a Lagrangian solver such as a finite element method), respectively. In this approach, the interaction between fluid and structure is achieved by applying respective boundary conditions to the individual solver separately. More specifically, the fluid is usually solved first with the structure assumed (unphysically) rigid, and then the structure is solved via imposing the force boundary conditions, which is obtained from the fluid solver, on the structure surface. The interface location obtained from the solid solver serves as the new boundary for the fluid solver in the next round of computation. If one intends to allow mesh along the interface, mesh regeneration has to be applied in the fluid domain at least in the vicinity of the interface. If the mesh is fixed for the fluid solver, special technique of treating irregular grid cells for the fluid solver is then required. The loose Euler-Lagrange coupling is relatively simple and convenient in numerical implementation. In addition, existing fluid and structure codes can be easily coupled together to simulate FSI problems. Current commercial software like ABACUS-FLUENT, ANSYS-CFX, LSDYNA commonly available in the market are built on the idea of using independent fluid and solid solvers. On the other hand, because of the weak and loose coupling, the boundary conditions at the interface for both fluid and structure are not imposed accurately (at least not at the same moment). Strictly speaking, the nonlinear (wave) interaction at the interface (the third issue mentioned above) is unable to be taken into consideration faithfully. In addition, numerical instability (the second issue mentioned above) is another problem frequently encountered.

The full Lagrange coupling involves a fully implicit monolithic approach where the fluid and the solid domains are solved simultaneously for the unknown variables; the interface boundary conditions are imposed as part of the solution and even the interface location is assumed to be part of the unknowns. This leads to the seamless coupling between the fluid domain and the solid domain. The full Lagrangian coupling usually leads to a large and complex numerical system, which requires iteration to obtain its solution with (possible) treatment of preconditioning [7]. Theoretically, on one hand, the nonlinear (wave) interaction at the interface can be captured faithfully using the full Lagrangian approach. On the other hand, the numerical instability is another major issue for this approach especially when the interface is under strong impact and large deformation. Furthermore, mesh regeneration is always required in the full Lagrangian coupling. The Arbitrary Euler-Lagrange (ALE) method is the

popular representative of this approach [8,20].

In recent years, an intermediate strategy, which tries to combine the advantages of the loose coupling and the full coupling, has become active. Among them, the ghost fluid method (GFM) [2,3,5,6] and the modified ghost fluid method (MGFM) [9, 11] are flexible and quite attractive. We call this type of approach as half-way Euler-Lagrange coupling. In the half-way approach, the fluid and the solid are separately solved by the respective Eulerian solver and Lagrangian solver like the loose coupling. However, there are obvious distinctions between the loose coupling and the half-way coupling. In the later, especially in the MGFM, the interface boundary conditions are accurately imposed and forced at the same moment. In addition, there are no irregular grid cells required for special treatment due to the definition of ghost cells and ghost fluids. In the MGFM, the nonlinear wave interaction at the interface is faithfully taken into account via constructing and solving a multi-medium Riemann problem. Such features built in the MGFM lead to robustness of the overall algorithm.

The MGFM has successfully applied to various gas-gas, gas-water and fluid-compressible solid problems [9, 11–13, 24, 26], where solid is modeled as fluid-like material under strong impact and governed by the Euler equations. In this work, the MGFM will be further developed to apply to the compressible fluid coupled to elastic solid. To model the elastic solid, the Navier equations based on the theory of elasticity for small deformation is employed. To take into account the influence of material deformation and nonlinear wave interaction at the interface, an Euler-Lagrange Riemann problem is constructed and solved at the interface along the normal direction. This work is an extension of the 1D method developed in [14] to multi-dimensions.

It may be noted that there are a few Euler-Euler couplings [15,21,23] for FSI when the structure is highly pressurized or under impact. In this work, only the Euler-Lagrange coupling is on focus.

The paper is organized as follows. In Section 2, the governing equations for both the fluid and solid media are presented; the 2D Navier equations are cast as a linear system similar to the Euler equations but in the Lagrangian coordinate. The Modified Ghost Fluid Method are developed and applied to treat the fluid-elastic solid interface in Section 3. Validation of the method is carried out in Section 4. Finally, a concluding summary is given in Section 5.

2 Governing equations

2.1 Governing equations for the fluid

The Euler equations for 2D compressible fluids can be written in a consistent form of

$$\frac{\partial U}{\partial t} + \frac{\partial F(U)}{\partial x} + \frac{\partial G(U)}{\partial y} = 0, \quad (2.1)$$

the respective expressions of U , F and G are given as

$$U = \begin{bmatrix} \rho \\ \rho u \\ \rho v \\ \rho E \end{bmatrix}, \quad F = \begin{bmatrix} \rho u \\ \rho u^2 + p \\ \rho uv \\ (E + p)u \end{bmatrix}, \quad G = \begin{bmatrix} \rho v \\ \rho uv \\ \rho v^2 + p \\ (E + p)v \end{bmatrix}.$$

Here ρ is the flow density, p is the pressure, u and v are the flow velocities in the x - and y - directions (Euler coordinates). E is the total energy and given as

$$E \equiv \rho e + 0.5\rho(u^2 + v^2),$$

where e is the internal energy per unit mass. For closure of System (2.1), an equation of state (EOS) is required. In the present study, the flow is assumed to be either compressible gas or compressible water. The EOS for compressible gas and water can be expressed in a consistent form of

$$\rho e = \frac{p}{\gamma - 1} + \frac{\gamma B}{\gamma - 1}. \quad (2.2)$$

Here γ and B are set to γ_g and zero for a gas medium, to γ_w and B_w , which are equal to 3.30E8Pa and 7.15, respectively, for water. The associated sound speed for EOS (2.2) can then be expressed as $c = \sqrt{\gamma \bar{p} / \rho}$, where $\bar{p} = p + B$.

2.2 Governing equations for two-dimensional solid

In many engineering applications, the solid structure is considered under linear elastic deformation, where the change of solid density is negligible and the structure motion is governed by the Navier equations written in the Lagrangian coordinates as [4]

$$(\lambda + 2\mu)\nabla(\nabla \cdot \vec{\epsilon}) - \mu\nabla \times (\nabla \times \vec{\epsilon}) - \rho_s \frac{\partial^2 \vec{\epsilon}}{\partial t^2} = \vec{f}. \quad (2.3)$$

Here

$$\lambda = \frac{\nu E}{(1 + \nu)(1 - 2\nu)} \quad \text{and} \quad \mu = \frac{E}{2(1 + \nu)},$$

are Lamé constants, E is Young's modulus and ν is the Poisson ratio. \vec{f} represents the body forces and is assumed to be zero in the present study and ϵ represents the displacement vector. The present interest is for two dimensions, Eq. (2.3) can then be written as

$$\rho_s \frac{\partial^2 \epsilon_1}{\partial t^2} = (\lambda + 2\mu) \frac{\partial^2 \epsilon_1}{\partial x'^2} + (\lambda + \mu) \frac{\partial^2 \epsilon_2}{\partial x' y'} + \mu \frac{\partial^2 \epsilon_1}{\partial y'^2}, \quad (2.4a)$$

$$\rho_s \frac{\partial^2 \epsilon_2}{\partial t^2} = (\lambda + 2\mu) \frac{\partial^2 \epsilon_2}{\partial y'^2} + (\lambda + \mu) \frac{\partial^2 \epsilon_1}{\partial x' y'} + \mu \frac{\partial^2 \epsilon_2}{\partial x'^2}, \quad (2.4b)$$

where ϵ_1 and ϵ_2 are displacements in the respective x' - and y' - directions (Lagrangian coordinates), ρ_s is the solid density. For isotropic elastic material, the stress-strain

relations are given by

$$\begin{bmatrix} \sigma_{x'x'} \\ \sigma_{y'y'} \\ \sigma_{x'y'} \end{bmatrix} = \begin{bmatrix} \lambda + 2\mu & \lambda & 0 \\ \lambda & \lambda + 2\mu & 0 \\ 0 & 0 & \mu \end{bmatrix} \begin{bmatrix} e_{x'x'} \\ e_{y'y'} \\ e_{x'y'} \end{bmatrix}, \tag{2.5a}$$

$$\begin{bmatrix} e_{x'x'} \\ e_{y'y'} \\ e_{x'y'} \end{bmatrix} = \begin{bmatrix} \frac{\partial \varepsilon_1}{\partial x'} \\ \frac{\partial \varepsilon_2}{\partial y'} \\ \frac{\partial \varepsilon_2}{\partial x'} + \frac{\partial \varepsilon_1}{\partial y'} \end{bmatrix}. \tag{2.5b}$$

If we define

$$u' = \frac{\partial \varepsilon_1}{\partial t} \quad \text{and} \quad v' = \frac{\partial \varepsilon_2}{\partial t},$$

as the particle velocity and on using (2.5), we can rewrite the governing equations (2.4) into stress-velocity form, which has a similar form to the Euler equations

$$\frac{\partial U'}{\partial t} + \frac{\partial F'(U')}{\partial x'} + \frac{\partial G'(U')}{\partial y'} = 0, \tag{2.6}$$

with

$$U' = \begin{bmatrix} \rho_s u' \\ \rho_s v' \\ -\sigma_{x'x'} \\ -\sigma_{y'y'} \\ -\sigma_{x'y'} \end{bmatrix}, \quad F'(U') = \begin{bmatrix} -\sigma_{x'x'} \\ -\sigma_{x'y'} \\ \alpha^2 \rho_s u' \\ (\alpha^2 - 2\beta^2) \rho_s u' \\ \beta^2 \rho_s v' \end{bmatrix}, \quad G'(U') = \begin{bmatrix} -\sigma_{x'y'} \\ -\sigma_{y'y'} \\ (\alpha^2 - 2\beta^2) \rho_s v' \\ \alpha^2 \rho_s v' \\ \beta^2 \rho_s u' \end{bmatrix}.$$

Here $\alpha = \sqrt{(\lambda + 2\mu)/\rho_s}$ and $\beta = \sqrt{\mu/\rho_s}$ are the wave speeds; $\sigma_{x'x'}$, $\sigma_{y'y'}$ and $\sigma_{x'y'}$ are the stress components; $e_{x'x'}$, $e_{y'y'}$ and $e_{x'y'}$ are the associated strain components. It can easily be proved that System (2.6) is hyperbolic.

3 The MGFM applied to Euler-Lagrange coupling

3.1 The outline of MGFM

In a MGFM-based algorithm for treating fluid-fluid coupling (i.e., Euler-Euler coupling), the Level Set technique [16] is usually employed to capture the moving material interface. A band of 3 to 5 grid points as ghost cells is defined in the vicinity of the material interface. At the ghost cells, ghost fluid and real fluid co-exist. To define ghost fluid states for the ghost cells, a multimedium Riemann problem is constructed and solved along the normal direction of material interface to predict the interface states; the predicted interface states are then employed to define the ghost fluid states. Once the ghost fluid nodes and ghost fluid states are defined for each medium, one employs one's favorite single medium numerical solver to solve for each medium covering both the real fluid and ghost fluid grid nodes next to the interface. By combining

the solution for each medium according to the new interface location, one then obtains the overall solution valid for the whole computational domain at the new time step.

When the MGFm is applied to treat the fluid-elastic solid coupling, there are several new aspects that have to be addressed because the governing equations for fluid are in the Eulerian coordinates with mesh fixed while the governing equations for solid are in the Lagrangian coordinates with moving grid nodes (mesh). One is how to define the ghost solid nodes for the solid in the Lagrangian coordinates (we named the ghost nodes used for computing the solid solution as (Lagrangian) ghost solid nodes); the second is how to construct and solve the fluid-solid Riemann problem at the fluid-solid interface and define ghost fluid/solid states, this is the core of MGFm; the third is how to advance the fluid-solid interface using the Level Set technique.

3.2 1D implementation

If we assume that the fluid and solid are located on the left and right sides of the interface, respectively, the coupled 1D fluid-solid (i.e., Euler-Lagrange) system can be expressed as

$$\begin{cases} \frac{\partial U}{\partial t} + \frac{\partial F}{\partial x} = 0, & \text{with } U|_{t=0} = U_0(x), \text{ for } x < x_0, \\ \frac{\partial U'}{\partial t} + \frac{\partial F'(U')}{\partial x'} = 0, & \text{with } U'|_{t=0} = U'_0(x'), \text{ for } x' > x'_0, \end{cases} \quad (3.1)$$

with

$$U' = \begin{bmatrix} \rho_s u' \\ -\sigma_{x'x'} \end{bmatrix}, \quad F'(U') = \begin{bmatrix} -\sigma_{x'x'} \\ \alpha^2 \rho_s u' \end{bmatrix}.$$

Here, x_0 is the initial interfacial location in the Eulerian system and its corresponding coordinate is denoted as x'_0 in the Lagrangian system. As shown in Fig. 1(a), there are respective mesh systems for fluid and solid computations, where they are allowed to overlap each other in the vicinity of the interface but their mesh nodes may not necessarily coincide with each other. In Fig. 1, the capital "I" indicates the Lagrangian nodes, while the small letter "i" stands for the Eulerian nodes; I_0 is the interface Lagrangian node. The mesh for the fluid domain is uniform, fixed and extended sufficiently into the solid domain for the purpose of advancing the Level Set function and constructing the fluid-solid (Euler-Lagrange) Riemann problem at the interface. The Lagrangian mesh for the solid is uniform only initially and moves with the local particle velocity. Those nodes (i.e., $i + 1$, $i + 2$ and $i + 3$ in Fig. 1(a)) extended into the solid medium serve as the ghost fluid nodes for computing fluid solution. The 1D Lagrangian ghost solid nodes are kept uniform and set to move with the predicted interface velocity. The locations of the Lagrangian ghost solid nodes, $I_0 - 1$ and $I_0 - 2$ as shown in Fig. 1(a), are determined using the formula,

$$x'_{I_0-1} = x'_{I_0} - \Delta x'_{I_0} \quad \text{and} \quad x'_{I_0-2} = x'_{I_0} - 2\Delta x'_{I_0},$$

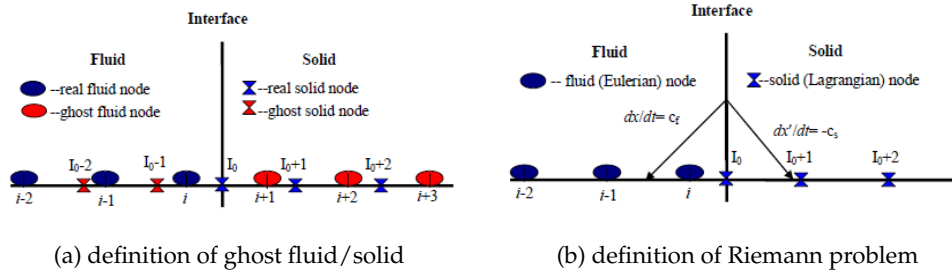


Figure 1: Illustration of the MGFM applied to 1D Euler-Lagrange coupling.

respectively. Here, x'_{I_0} is the interface Lagrangian coordinate and $\Delta x'_{I_0} = x'_{I_0+1} - x'_{I_0}$. The most important feature of the MGFM is the construction of a fluid-solid Riemann problem at the interface to take into consideration the fluid-solid nonlinear interaction. Assuming that the solution is known at $t = t^n$ and we want to obtain the solution at $t = t^{n+1}$ for the 1D Euler-Lagrange System (3.1), the fluid-solid (Euler-Lagrange) Riemann problem to be constructed at the interface can be expressed as

$$\begin{cases} \frac{\partial U}{\partial t} + \frac{\partial F}{\partial x} = 0, & \text{with } U|_{t=t^n} = U_{IL}, \text{ for } x < x'_I, \\ \frac{\partial U'}{\partial t} + \frac{\partial F'(U')}{\partial x'} = 0, & \text{with } U'|_{t=t^n} = U'_{IR}, \text{ for } x' > x'_I. \end{cases} \quad (3.2)$$

Here, x'_I is the interface location in the Eulerian coordinates at $t = t^n$ and x''_I is its associated Lagrangian coordinate. There are several ways of obtaining U_{IL} and U'_{IR} . One of the ways is via interpolation along the two non-linear characteristic lines tracing back from the interface into the respective fluid and solid media as shown in Fig. 1(b). In the present study, fluid state at node $i - 1$ and solid state at $I_0 + 2$ as shown in Fig. 1(b) are simply set to be U_{IL} and U'_{IR} , respectively. System (3.2) might exactly be solved to obtain the interface state in some special situations [14]. Here, we introduce an approximate way of solving System (3.2) for general applications by taking advantage of the two characteristics, which intersect at the interface from the fluid and solid domains, respectively. One can easily find that there is a positive characteristic and a negative characteristic intersecting at the interface, respectively, from the fluid and solid domains. These are

$$\frac{dp_I}{dt} + \rho_{IL} c_{IL} \frac{du_I}{dt} = 0, \quad \text{along } \frac{dx}{dt} = u_I + c_{IL}, \quad (3.3a)$$

$$\frac{du'_I}{dt} - \frac{c_s}{E} \frac{d\sigma_I}{dt} = 0, \quad \text{along } \frac{dx'}{dt} = -c_s. \quad (3.3b)$$

Here, $c_s = \alpha$. The following approximate Riemann problem solver is employed to solve System (3.3) as suggested in [14]

$$\frac{p_I - p_{IL}}{W_I} + (u_I - u_{IL}) = 0, \quad W_I = \sqrt{\frac{p_I - p_{IL}}{\rho_{IL}^{-1} - (\rho_I(p_I))^{-1}}}, \quad (3.4a)$$

$$u'_I - \frac{c_s}{E} \sigma_I = u'_{IR} - \frac{c_s}{E} \sigma_{IR}. \quad (3.4b)$$

Here, subscripts "I", "IL" and "IR" refer to the interface, the left and right sides of the interface, respectively. u_I (u'_I) and p_I (σ_I) are the velocity and pressure (stress) at the interface, where $\sigma_I = p_I$ and $u_I = u'_I$ (here, tension is defined as negative in one dimension).

System (3.4) has to be solved via iteration. Once the interface pressure and velocity are obtained via solving (3.4), the interface density for fluid can be obtained using the equation of state. The predicted interface states are then employed to define the ghost fluid states and the ghost solid states, respectively. More specifically, (ρ_I, u_I, p_I) are used to define the ghost fluid density, velocity and pressure at ghost nodes, $i + 1$ and $i + 2$ shown in Fig. 1(a). (u'_I, σ_I) are used to define the ghost solid velocity and stress at ghost nodes $I_0 - 1$ and $I_0 - 2$. For robustness of computation under the lower pressure situation, the real-ghost fluid method (rGFM)-like version [24] is suggested to treat the solid side, where (u'_I, σ_I) are also used to define the boundary conditions at node I_0 and the ghost solid velocity and stress at ghost solid nodes.

To advance the interface, the following level set equation in the Eulerian coordinate is solved in the vicinity of the interface with the ghost fluid nodes included

$$\frac{\partial \phi}{\partial t} + u_I \frac{\partial \phi}{\partial x} = 0. \quad (3.5)$$

To update the Lagrangian mesh for the solid, we employ following method for the interface motion equation

$$\frac{dx'_I}{dt} = u'_I, \quad x'^{n+1}_I = x'^n_I + 0.5(u'^{n+1}_I + u'^n_I)\Delta t. \quad (3.6)$$

Assuming at $t = t^n$ that the solution is known and the interface is located between nodes i and $i + 1$ in the Eulerian mesh, below we summarize the general procedure of the MGFm-based algorithm when applied to the 1D Euler-Lagrange computation to obtain the solution at $t = t^{n+1}$ with the time stepsize of $\Delta t = \min\{\Delta t_f, \Delta t_s\}$. where Δt_f and Δt_s are time stepsizes for the respective fluid and solid computations due to stability constraints.

1. Construct the Euler-Lagrange Riemann problem at the material interface via setting

$$U_{IL} = U_{i-1} \quad \text{and} \quad U'_{IR} = U'_{I_0+2},$$

and solve the Euler-Lagrange Riemann problem approximately via (3.4) to obtain the respective interface fluid and solid states, (ρ_I, u_I, p_I) and (u'_I, σ_I) .

2. Set the convect velocity of Level Set as u_I in the band of, say, $|\phi^n| \leq 3.5\Delta x$ (i.e., define the extension velocity field for motion of the Level Set) and advance the interface via solving the Level Set equation (3.5) to the new time step, and get the new interface location.
3. Define the ghost fluid states as (ρ_I, u_I, p_I) for ghost fluid at ghost nodes $i + 1$ and $i + 2$ and solve for the fluid medium from grid 1 to grid $i + 1$ using the numerical solver suitable for the fluid.

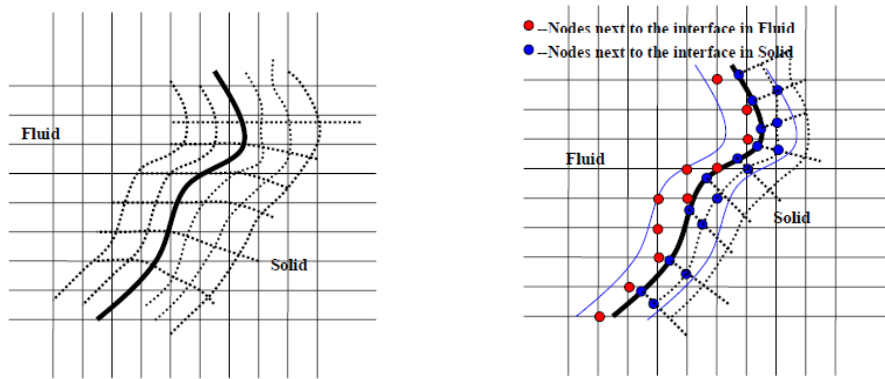
4. Define ghost solid nodes x'_{I_0-1} , x'_{I_0-2} and define ghost solid states as (u'_I, σ_I) for the ghost solid at ghost solid nodes.
5. Solve for the solid medium using the numerical solver suitable for the solid from node $I_0 - 1$ to the end of solid domain and update the Lagrangian mesh for the solid via (3.6).
6. Obtain the final solution over whole computation domain at the new time step according to the new interface location.
7. Update the new time step size and go back to Step 1 and proceed to the next time step.

3.3 2D implementation

By using the present technique in the normal direction of the interface, the MGFm can be implemented for multi-dimensions. However, there are relatively more involved because different coordinate systems are used for the fluid and solid media. Special treatments are also required for the interface tangential velocity and interface tangential stress for the solid. Again, even as the respective mesh systems for fluid and solid computations are employed, both meshes are allowed to overlap each other in the vicinity of the interface but they may not necessarily coincide with each other. The Eulerian mesh for fluid computation is fixed, uniform and extended sufficiently into the solid domain; the Lagrangian mesh for solid moves with the local velocity with at least one layer of ghost solid nodes extended into the fluid domain (see Fig. 2). The level set function is defined over the fluid mesh including ghost fluid nodes. To advance the interface, the level set equation with the extension velocity field [1, 24] is solved in the Eulerian coordinate in a band next to the interface:

$$\frac{\partial \phi}{\partial t} + u_n |\nabla \phi| = \frac{\partial \phi}{\partial t} + u_n \vec{n} \cdot \nabla \phi = 0. \tag{3.7}$$

Here, $\vec{n} = \nabla \phi / |\nabla \phi|$, $u_n \vec{n}$ is the extension velocity field. To obtain the extension velocity, the predicted interface velocity is extended to all the grid nodes inside the band (see Subsection 3.3.1 for more details). Once the extension velocity field is defined, one uses his/her favourite level set solver to advance the level set function (a signed distance function). In 1D computation, it is easy to maintain the interface as a Lagrange node. However, it is quite troublesome to keep on maintaining the initial Lagrange nodes on the moving interface, especially when the interface is under large deformation. In this work, we employ the level set technique to capture the interface; this might result in the initial Lagrange nodes on the interface shifting away from the interface, and the interface does not take on or assume the Lagrange nodes any more. Because of the employment and definition of ghost solid nodes, one will however find that the treatment of the interface inside the solid domain becomes relatively easy under the framework of MGFm. The general strategy of treating the interface using MGFm follows two steps: 1) constructing and solving an Euler-Lagrange Riemann



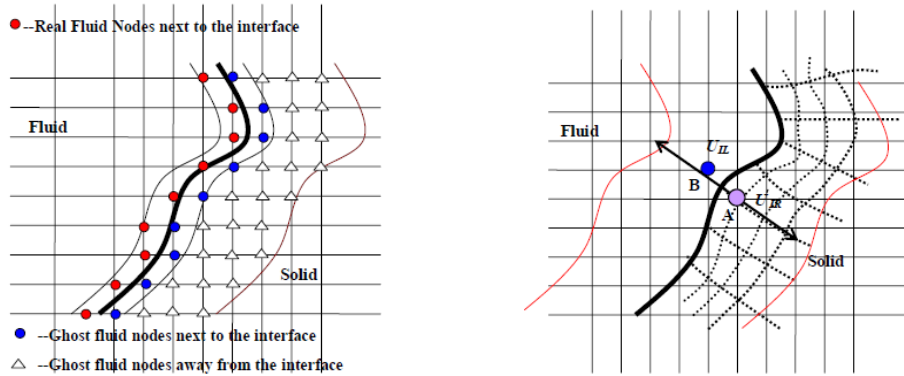
(a) Overlapped Eulerian/Lagrangian mesh (b) Eulerian/Lagrangian nodes next to interface

Figure 2: Illustration of Mesh for Fluid and Solid Domains (The solid lines are Eulerian grids; the dotted curves are Lagrangian grids; the bold line is the interface).

problem at each ghost fluid/solid nodes just next to the interface along the normal direction, 2) propagating the predicted interface states to those ghost fluid/solid nodes away from the interface.

3.3.1 Definition of ghost fluid state

Firstly, we shall present the procedure of defining the Riemann problem for treating the ghost fluid nodes. With the help of level set function, we can define a band of 2 to 4 grid points via $|\phi| < \eta$ in the vicinity of the interface under the Eulerian mesh background. Here η is set to be about $3 \min(\Delta x, \Delta y)$ to $5 \min(\Delta x, \Delta y)$; Δx and Δy are the spatial step sizes in the respective x - and y - directions. We divide the grid points in the band into three subsets for the fluid, Ω_{η}^{F-Real} , $\Omega_{\eta}^{GF-Near}$ and Ω_{η}^{GF-far} . Ω_{η}^{F-Real} consists of the real fluid nodes next to the interface inside the band; $\Omega_{\eta}^{GF-Near}$ includes the ghost fluid points just next to the interface; Ω_{η}^{GF-far} consists of other ghost fluid points in the band. Fig. 3(a) illustrates the elements included in the sets of Ω_{η}^{F-Real} , $\Omega_{\eta}^{GF-Near}$ and Ω_{η}^{GF-far} . Ω_{η}^{F-Real} includes the grid nodes indicated with "red circles" on the left side of the interface in the band. $\Omega_{\eta}^{GF-Near}$ includes the grid nodes indicated with "blue circles" on the right side of the interface inside the solid domain as shown in Fig. 3(a). Ω_{η}^{GF-far} comprises the grid nodes indicated with "triangles" inside the solid domain as depicted in Fig. 3(a). We first construct and solve an Euler-Lagrange Riemann problem at each ghost fluid node in the set of $\Omega_{\eta}^{GF-Near}$. Considering a ghost fluid node **A** (the "purple circle" in Fig. 3(b)), which is just bordering the interface in the solid, we search for another node **B** (the "blue circle" in Fig. 3(b)), which also borders the interface but inside the fluid such that the angle made by the respective normals at node **A** and node **B** is the minimum. We use the fluid state, U_{IL} , at node **B** and solid state, U'_{IR} , at **A** to construct a 1D Euler-Lagrange Riemann problem to obtain the ghost fluid state U^*_{IR} at this point (note that interpolation is usually required



(a) elements in sets of Ω_{η}^{F-Real} , $\Omega_{\eta}^{GF-Near}$ and Ω_{η}^{GF-far} (b) definition of Riemann problem

Figure 3: Illustration of the MGFM to define ghost fluid state (bold line is the interface).

to obtain the solid state at node **A** because node **A** may not take a solid Lagrangian node). More specifically, by projecting the respective velocity fields at nodes **A** and **B** and the stress at node **A** into the normal direction and tangential direction at node **A**, we have $\vec{u}_{IL} = u_{IL,n}\vec{n}_{IR} + u_{IL,\tau}\vec{\tau}_{IR}$, $\vec{u}'_{IL} = u'_{IR,n}\vec{n}_{IR} + u'_{IR,\tau}\vec{\tau}_{IR}$, $\sigma_{IR,n'n'}$, $\sigma_{IR,\tau'n'}$ and $\sigma_{IR,\tau'\tau'}$. Here

$$\vec{n}_{IR} = [n_{IR,x} \ n_{IR,y}]^T,$$

is the unit normal vector at node **A**, which can be calculated using

$$\vec{n}_{IR} = \nabla\phi_A|\nabla\phi_A|^{-1},$$

and

$$\vec{\tau}_{IR} = [\tau_{IR,x} \ \tau_{IR,y}]^T,$$

is the counterpart tangential vector, and

$$\sigma_{IR,n'n'} = n_{IR,x}^2\sigma_{IR,x'x'} + 2n_{IR,x}n_{IR,y}\sigma_{IR,x'y'} + n_{IR,y}^2\sigma_{IR,y'y'}, \tag{3.8a}$$

$$\sigma_{IR,\tau'\tau'} = \tau_{IR,x}^2\sigma_{IR,x'x'} + 2\tau_{IR,x}\tau_{IR,y}\sigma_{IR,x'y'} + \tau_{IR,y}^2\sigma_{IR,y'y'}, \tag{3.8b}$$

$$\sigma_{IR,\tau'n'} = \tau_{IR,x}n_{IR,x}\sigma_{IR,x'x'} + (\tau_{IR,x}n_{IR,y} + n_{IR,x}\tau_{IR,y})\sigma_{IR,x'y'} + \tau_{IR,y}n_{IR,y}\sigma_{IR,y'y'}. \tag{3.8c}$$

$\sigma_{IR,x'x'}$, $\sigma_{IR,x'y'}$ and $\sigma_{IR,y'y'}$ are the respective stress components at node **A**. We can form a 1D Euler-Lagrange Riemann problem with its initial states as $U'_{IR,n}$ and $U_{IL,n}$ at node **A**. Here,

$$U'_{IR,n} = [\rho_s u'_{IR,n} \ -\sigma_{IR,n'n'} \ -\sigma_{IR,\tau'\tau'}]^T \quad \text{and} \quad U_{IL,n} = [\rho_{IL} \ \rho_{IL} u_{IL,n} \ E_{IL,n}]^T,$$

with

$$E_{IL,n} = \rho_{IL} e_{IL} + 0.5\rho_{IL} u_{IL,n}^2.$$

That is

$$\begin{cases} \frac{\partial U_n}{\partial t} + \frac{\partial F_n(U_n)}{\partial n} = 0, & \text{with } U|_{t=t^n} = U_{IL,n} \text{ on the left,} \\ \frac{\partial U'_n}{\partial t} + \frac{\partial F'_n(U'_n)}{\partial n'} = 0, & \text{with } U'|_{t=t^n} = U'_{IR,n} \text{ on the right,} \end{cases} \quad (3.9)$$

with

$$\begin{aligned} U_n &= [\rho \ \rho u_n \ E_n]^T, & F_n(U_n) &= [\rho u_n \ \rho u_n^2 + p \ (E_n + p)u_n]^T, \\ U'_n &= [\rho_s u'_n \ -\sigma_{n'n'} \ -\sigma_{\tau'\tau'}]^T, & F'_n(U'_n) &= [-\sigma_{n'n'} \ \alpha^2 \rho_s u'_n \ (\alpha^2 - 2\beta^2)\rho_s u'_n]^T. \end{aligned}$$

We then solve this Riemann problem using formula (3.13) to be given below in Sub-section 3.3.3. The density can be obtained via the fluid EOS. The predicted pressure, p_I , and density, ρ_I , are used to define the pressure and density of ghost fluid status at node **A**, i.e.,

$$p_{IR}^* = p_I \quad \text{and} \quad \rho_{IR}^* = \rho_I.$$

The ghost fluid velocity at this point is the vector summation of the predicted normal velocity, $u_{I,n}\vec{n}_{IR}$ and the local tangential velocity $u_{IL,\tau}\vec{v}_{IL}$ at node **B**, i.e.,

$$\vec{u}_{IR}^* = u_{I,n}\vec{n}_{IR} + u_{IL,\tau}\vec{v}_{IL}.$$

Thus the ghost fluid status at node **A** is defined.

Once the ghost fluid states for all points in the set of $\Omega_\eta^{GF-Near}$ are defined, the next step is to define the ghost fluid states for other ghost fluid points in the set of Ω_η^{GF-far} . This is done via solving

$$U_\nu \pm \vec{n} \cdot \nabla U = 0,$$

to steady state with fluid states fixed at grid nodes in both Ω_η^{F-Real} and $\Omega_\eta^{GF-Near}$; if ϕ is negative in the real fluid side, $U_\nu + \vec{n} \cdot \nabla U = 0$ is solved, otherwise $U_\nu - \vec{n} \cdot \nabla U = 0$ is solved. Solving $U_\nu \pm \vec{n} \cdot \nabla U = 0$ to steady state is very fast by a first-order upwind scheme. It should be noted that once the ghost fluid states are defined in the band, the Level Set extension velocity field is obtained and then the Level Set function can be advanced to the next time step over the Eulerian mesh in the band.

3.3.2 Definition of ghost solid state

Defining ghost solid nodes and ghost solid states are much more involved in the moving and deformable Lagrangian mesh. Unlike the definition of ghost solid nodes in one dimension, where they are kept uniformly by redefining them at each time step, the redefinition of ghost solid nodes is troublesome in multi-dimensions at each time. To avoid this trouble, the ghost solid nodes are defined initially during the mesh generation of solid domain and allowed to move with the predicted "interface" velocity in multi-dimensions to be described in more details late. Similarly, we define Ω_η^{S-Real} , $\Omega_\eta^{GS-Near}$ and Ω_η^{GS-far} for treating the ghost solid nodes. Ω_η^{S-Real} consists of the real

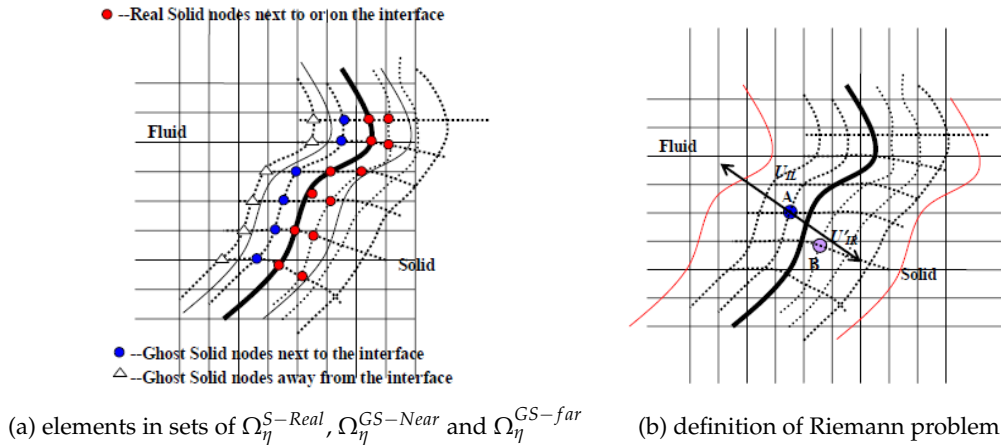


Figure 4: Illustration of the MGFM to define ghost solid state (bold line is the interface).

solid nodes next to and on the interface inside the band (the "red circles" in Fig. 4(a)); $\Omega_{\eta}^{GS-Near}$ includes the ghost solid points just next to the interface (the "blue circles" in Fig. 4(a)); Ω_{η}^{GS-far} consists of other ghost solid points in the band (the "triangles" in Fig. 4(a)). We first define an Euler-Lagrange Riemann problem for each ghost solid node in the set of $\Omega_{\eta}^{GS-Near}$. Assuming that node **A** is a ghost solid (the "blue circle" in Fig. 4(b)) just bordering the interface inside the fluid domain, we search for a counterpart node **B** (the "purple circle" in Fig. 4(b)) in the solid domain such that the angle made by the respective normals at node **A** and node **B** is the minimum. Because level set function is defined on the fixed Eulerian rectangular mesh, nodes **A** and **B** may not be Eulerian nodes, interpolation is required to obtain the respective normals at nodes **A** and **B**. By projecting the respective velocity fields at nodes **A** and **B** and the stress at node **B** into the normal direction and tangential direction, we can use the fluid state, U_{IL} , at node **A** and the solid state, U'_{IR} , at node **B** to construct an 1D Euler-Lagrange Riemann problem along the normal direction of node **A** with the initial states of $U_{IL,n}$ and $U'_{IR,n}$ (similar to (3.9)). It should be noted that interpolation is again usually required to obtain the fluid state at node **A** during the construction of the Riemann problem because **A** may not be at an Eulerian node. We solve this Riemann problem via the approach (3.13) presented in Subsection 3.3.3 to obtain the interface normal velocity $u'_{I,n}$, the normal stress component $\sigma_{I,n'n'}$. The predicted $\sigma_{I,n'n'}$ and $u'_{I,n}$ are used to define the normal stress component and normal velocity component of the ghost solid state at node **A**. The ghost solid velocity at this point is the vector summation of the predicted normal velocity, $u'_{I,n} \vec{n}_{IR}$ and the local tangential velocity $u'_{IL,\tau} \vec{\tau}_{IL}$ at node **B**. Thus the ghost solid velocity at node **A** is defined. To define the ghost solid stress at node **A**, besides the normal stress component $\sigma_{I,n'n'}$ we still need to define the tangential stress component $\sigma_{I,\tau'\tau'}$ and the cross shear stress component $\sigma_{I,\tau'n'}$. The cross shear stress component is approximately obtained with the local cross shear stress component $\sigma_{IR,\tau'n'}$ at node **B**. The computation of the tangential stress component $\sigma_{I,\tau'\tau'}$ is given in Subsection 3.3.3.

Defining ghost solid states for the ghost solid points in the set of Ω_η^{GS-far} is not necessary because the defined ghost solid states for the points in the set of $\Omega_\eta^{GS-Near}$ can serve as approximate boundary conditions for the solid. For robustness of computation under the lower pressure situation, the rGFM [24] can be applied, where an Euler-Lagrange Riemann problem is defined and solved to predict the solid states for those real solid nodes just next to and on the interface. With the definition of ghost solid states in $\Omega_\eta^{GS-Near}$, their motion and locations can be determined in the next time. They can then serve as the ghost solid nodes in the next round of computation as well.

3.3.3 Solve the Euler-Lagrange Riemann problem

Once the Euler-Lagrange Riemann problem is constructed along the normal direction, we need to (approximately) solve it to predict the normal velocity, the normal stress component, the tangential stress component. To develop an approximate Riemann solver for System (3.9), we again take advantage of the characteristic equations of System (3.9). The characteristic equations for the fluid equations of System (3.9) are

$$\begin{cases} \frac{dp}{dt} - \rho c \frac{du_n}{dt} = 0, & \text{along } \frac{dn}{dt} = u_n - c, \\ \frac{dp}{dt} - c^2 \frac{d\rho}{dt} = 0, & \text{along } \frac{dn}{dt} = u_n, \\ \frac{dp}{dt} + \rho c \frac{du_n}{dt} = 0, & \text{along } \frac{dn}{dt} = u_n + c. \end{cases} \quad (3.10)$$

The characteristic equations for the solid equations of System (3.9) are

$$\begin{cases} \frac{du'_n}{dt} - \frac{1}{\rho_s \alpha} \frac{d\sigma_{n'n'}}{dt} = 0, & \text{along } \frac{dn'}{dt} = -c_s, \\ \frac{d\sigma_{\tau'\tau'}}{dt} - \frac{(\alpha^2 - 2\beta^2)}{\alpha^2} \frac{d\sigma_{n'n'}}{dt} = 0, & \text{along } \frac{dn'}{dt} = 0, \\ \frac{du'_n}{dt} + \frac{1}{\rho_s \alpha} \frac{d\sigma_{n'n'}}{dt} = 0, & \text{along } \frac{dn'}{dt} = c_s. \end{cases} \quad (3.11)$$

From (3.10) and (3.11), the two characteristics intersecting at the interface respectively from the fluid and solid domains are

$$\frac{dp_I}{dt} + \rho_{IL} c_{IL} \frac{du_{I,n}}{dt} = 0, \quad \text{along } \frac{dn}{dt} = u_{I,n} + c_{IL}, \quad (3.12a)$$

$$\frac{du'_{I,n}}{dt} - \frac{1}{\rho_s c_s} \frac{d\sigma_{I,n'n'}}{dt} = 0, \quad \text{along } \frac{dn'}{dt} = -c_s. \quad (3.12b)$$

We can similarly solve System (3.12) as in (3.4)

$$\frac{p_I - p_{IL}}{W_I} + (u_{I,n} - u_{IL,n}) = 0, \quad W_I = \sqrt{\frac{p_I - p_{IL}}{\rho_{IL}^{-1} - (\rho_I(p_I))^{-1}}}, \quad (3.13a)$$

$$u'_{I,n} - \frac{1}{\rho_s c_s} \sigma_{I,n'n'} = u'_{IR,n} - \frac{1}{\rho_s c_s} \sigma_{IR,n'n'}. \quad (3.13b)$$

We then obtain the interface pressure, normal velocity and normal stress via solving (3.13). To obtain the interface tangential stress, we integrate the second equation of (3.11) and have

$$\sigma_{I,\tau'\tau'} = \frac{\alpha^2 - 2\beta^2}{\alpha^2} \sigma_{I,n'n'} + \sigma_{IR,\tau'\tau'} - \frac{\alpha^2 - 2\beta^2}{\alpha^2} \sigma_{IR,n'n'}. \tag{3.14}$$

Thus, we can completely define the solid stress at the ghost solid nodes with $\sigma_{I,n'n'}$, $\sigma_{I,\tau'\tau'}$ and $\sigma_{I,\tau'n'}$.

Assuming that the fluid and solid computational domains have been meshed initially with sufficient ghost fluid grids extended into the solid domain and at least one layer of ghost solid nodes extended into the fluid domain, and that the solution and interface are known at $t = t^n$, below we summarize the general procedure of the MGFm-based algorithm when applied to the two-dimensional Euler-Lagrange computation as follows

1. Define a band of $|\phi^n| < \eta$ and obtain Ω_η^{F-Real} , $\Omega_\eta^{GF-Near}$, Ω_η^{GF-far} , Ω_η^{S-Real} , $\Omega_\eta^{GS-Near}$ and Ω_η^{GS-far} .

2. Define the ghost fluid states at each ghost fluid node in the set of $\Omega_\eta^{GF-Near}$ and then define the ghost fluid states for those ghost fluid points in the set of Ω_η^{GF-far} by solving

$$U_{t'} + \vec{n} \cdot \nabla U = 0 \quad \text{or} \quad U_{t'} - \vec{n} \cdot \nabla U = 0,$$

to steady state with fluid states fixed at grid nodes in both Ω_η^{F-real} and $\Omega_\eta^{GF-Near}$.

3. Solve for fluid solution over the whole fluid domain with the ghost fluid nodes in $\Omega_\eta^{GF-Near}$ included.
4. Advance the level set function ϕ to the next time step in the band and identify the fluid domain and solid domain using level set function at the new time (i.e., the new interface location).
5. Define ghost solid states for those ghost solid nodes in the set of $\Omega_\eta^{GS-Near}$.
6. Solve for the solid medium to the new time step with the ghost fluid nodes in $\Omega_\eta^{GS-Near}$ included.
7. Update the Lagrangian mesh for the solid including those ghost solid nodes in $\Omega_\eta^{GS-Near}$.
8. Obtain the final solution over whole computation domain at the new time step according to the new interface location.
9. Update the new time step size, go back to Step 1 and proceed to the next time step.

4 Numerical results

In this section, several problems are used to test the method developed in Section 3. All the computations are carried out via the 2D MUSCL scheme [22, 25]. Except for explicit statement mentioned, all parameters are non-dimensional with $\rho_{ref} = 1000\text{kg/m}^3$, $p_{ref} = 1.0 \times 10^5\text{Pa}$, $L_{ref} = 1.0\text{m}$, $u_{ref} = \sqrt{p_{ref}/\rho_{ref}} = 10.0\text{m/s}$ and $t_{ref} = L_{ref}/u_{ref} = 0.1\text{s}$. Here, ρ_{ref} , p_{ref} , L_{ref} , u_{ref} and t_{ref} are the reference density, pressure, length, velocity and time. The material for the solid is chosen to be stainless steel, AISI 431 with the mechanical properties shown in Table 1. The problems selected in this work are very tough and may not work out for other methods like a fully coupled Euler-Lagrange method, even for a loose coupled Euler-Lagrange method. The present method, however, performs consistently.

Table 1: Properties of AISI 431 Stainless Steel (SI unit) for 200°C.

Density ρ (Kg/m ³)	Young's Modulus (GPa)	Tensile Strength (Mpa)	Poisson Ratio	Bulk Modulus (Gpa)	Shear Modulus (Gpa)
7.7	215.116	850-1000	0.283	166.16	166.16

Case 4.1. This is a 1D gas-solid Euler-Lagrange Riemann problem, where a high pressurized gas jet impacts on the solid. The non-dimensional initial conditions are $u_l = 50.0$, $p_l = 10000.0$, $\rho_l = 0.05$, $\gamma_l = 1.4$; $u_r = 0.0$, $p_r = 1.0$, $\rho_r = 7.7$. The computational domain is $[0, 10]$ with 2200 grids. The initial location of the interface is at 5.0. The CFL is set at 0.8. Fig. 5(a) and (b) show the velocity, pressure and stress distribution in the gas and the solid medium at $t = 4.45E - 3$, which are in good agreement with the analytical (exact) solution.

Case 4.2. A water jet heads on a moving steel solid horizontally. This is essentially a 1D water-solid Euler-Lagrange Riemann problem but computed using the 2D Navier equation with the computational domain set to be $x \times y \in [0, 10] \times [0, 10]$ and 2200×10

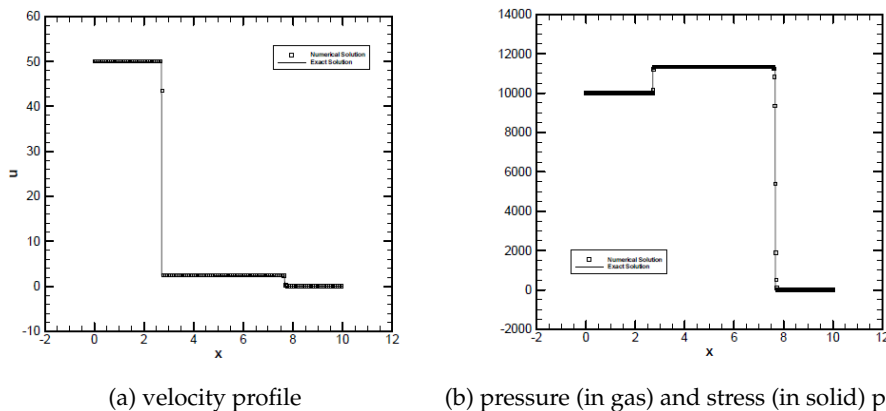


Figure 5: The velocity and pressure/normal stress profiles for Case 4.1.

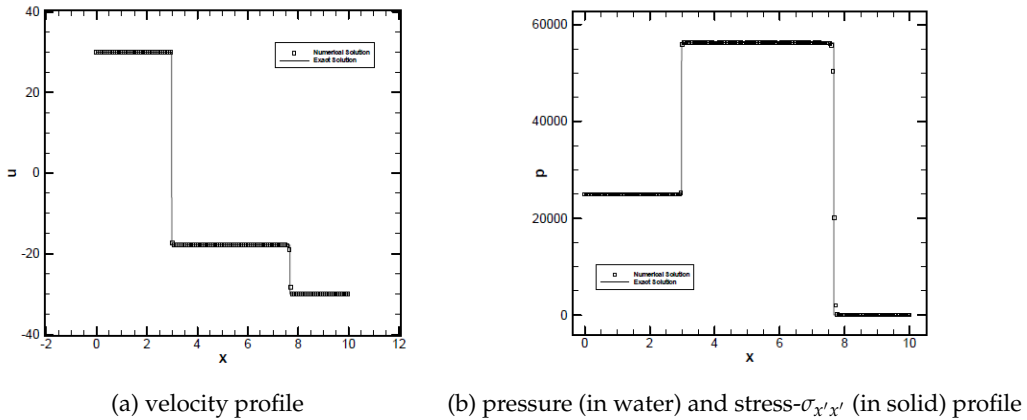


Figure 6: The velocity and pressure/normal stress profiles for Case 4.2.

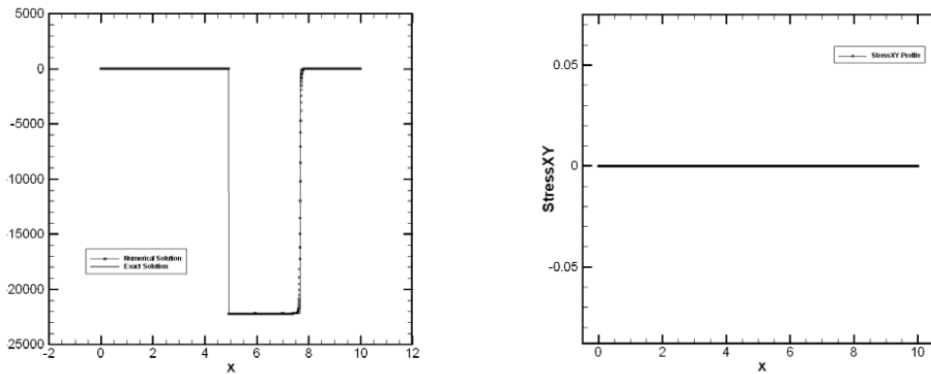
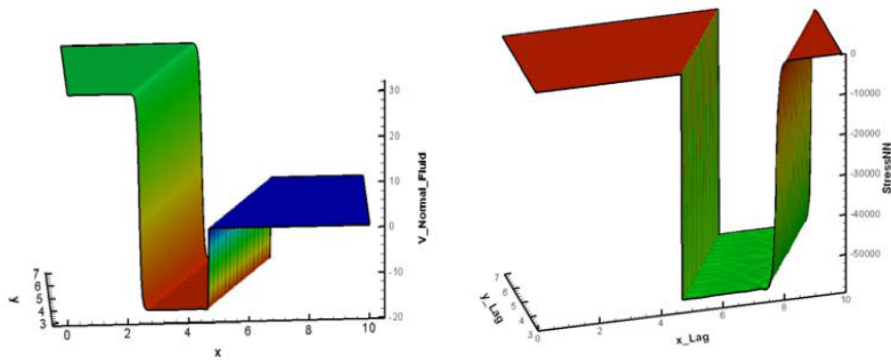


Figure 7: The tangential (StressYY) and shear stress (StressXY) profiles for Case 4.2.

uniform grids used. The employment of 2D Navier equation for the solid leads to the presence of tangential stress $\sigma_{y'y'}$, while the shear stress is zero everywhere in the solid medium. The non-dimensional initial conditions are $u_l = 30.0, v_l = 0.0, p_l = 25000.0; u_r = -30.0, v_r = 0.0, p_r = 1.0$. The initial location of the interface is at $(5.0, 0.0)$ with $CFL = 0.8$. In this case shock waves are generated that moves respectively through the water to the left and the solid to the right. Fig. 6(a) and (b) show the velocity, respective pressure and stress $-\sigma_{x'x'}$ distribution in the water and the solid medium at $t = 4.45E - 3$. The numerical results show good agreement with the analytical (exact) solution. Fig. 7(a) and (b) show the associated tangential stress $\sigma_{y'y'}$ (StressYY) and shear stress $\sigma_{x'y'}$ (StressXY) profiles, which also coincide with the exact solution very well. In the plots of tangential and shear stresses, they are set to be zero in the fluid domain.

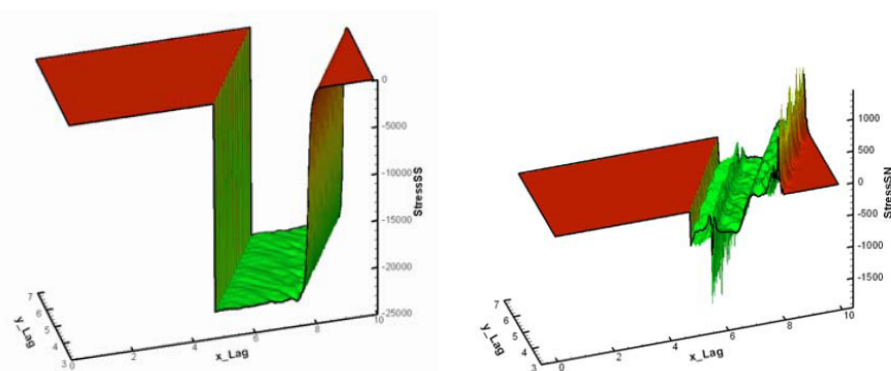
Case 4.3. This case is the same as Case 4.2 except with an anticlockwise coordinate rotation of 60° and 251×251 uniform mesh is employed. The CFL is set to 0.4 in computation. This setup results in the fluid-structure interface never coincides with the interface, and treatment of the interface and computation are fully in two dimensions.



(a) velocity contours in fluid

(b) normal stress contours in solid

Figure 8: The normal velocity in fluid and normal stress in solid for Case 4.3.



(a) tangential stress contours in solid

(b) shear stress contours in solid

Figure 9: The tangential (StressSS) and shear stress (StressSN) contours for Case 4.3.

In order to make comparison to the results of Case 4.2, the plotted numerical results of velocity and stresses are transferred to the interface normal direction. Fig. 8(a) and (b) show the normal velocity (V_Normal_Fluid) in the fluid (where the velocity in the solid domain is set to zero), the normal stress ($StressNN$) in the solid at $t = 4.45E - 3$. Both the shock wave locations and the magnitude of velocity and pressure (normal stress) are in good agreement with Case 4.2. In addition, the associated tangential stress ($StressSS$) and shear stress ($StressSN$) are shown in the respective Fig. 9(a) and (b). Theoretically, the shear stress should be zero for this case. Because the shock front does not coincide with the Lagrange mesh lines, this results in a non-zero shear stress behind the shock front in the solid. Fig. 9(b) clearly exhibits that the shear stress starts oscillations just from the shock front, while it ensures a correct zero value at the interface. The magnitude of the shear stress, however, is only about 5% of the magnitude of the corresponding normal stress and kept in a very reasonable level. In fact, it is very difficult to completely eliminate these undesirable oscillations once the shock front is not along a mesh line due to the coupling of stress components through constitution relations. In the plots of stress, the stress is set to zero in the fluid domain.

Case 4.4. Underwater Explosion. In this case, a series of shock wave and rarefaction wave acts and reflects on the water-solid interface and the water cavitates near the structure. Hence, this benchmark problem can best identify the weakness and strength of the present solver. The initiation of explosion is avoided by considering the explosive bubble to be a high pressure zone containing ideal gas of high density initially and located at the origin (0.0m, 0.0m) with radius 1.0m. Water at atmospheric pressure surrounds the high pressure bubble. The solid wall is a semi-infinite elastic solid taking on a straight interface (parallel to the y -axis) with the water medium at $x = 3.025\text{m}$ initially. The computational domain is a square of dimension $12\text{m} \times 12\text{m}$. Fig. 10 shows the definition of the problem schematically. The bottom left corner of the computational domain is at $(-6\text{m}, -6\text{m})$ and the upper right corner is at $(6\text{m}, 6\text{m})$. The initial conditions for the materials involved are as follows:

$$\begin{aligned} \text{Explosive Gas :} \quad & p_{gas} = 8290 \times 10^5 \text{Pa}; \quad \rho_{gas} = 1.27 \times 10^3 \text{Kg/m}^3; \quad \gamma = 2.0. \\ \text{Water :} \quad & p_{water} = 1.0 \times 10^5 \text{Pa}; \quad \rho_{water} = 1.0 \times 10^3 \text{Kg/m}^3. \\ \text{Elastic Solid :} \quad & \sigma_{x'x'} = -1.0 \times 10^5 \text{Pa}; \quad \sigma_{x'y'} = 0.0 \text{Pa}; \quad \sigma_{y'y'} = 0.0 \text{Pa}. \end{aligned}$$

The initial velocity for each of the medium is zero, i.e., $u = 0; v = 0$. The number of grid divisions employed is 361×361 with $CFL = 0.4$.

The pressure distribution in the water and gas and the stress distribution for the x' -component, i.e., $\sigma_{x'x'}$ in the elastic solid at different instances are displayed in Fig. 11(a) to (c). Fig. 11(a) shows that the shock wave generated by the explosive bubble, which we call the "main shock", has reflected back and moving towards the bubble (we call this the "1st reflected shock wave") at $t = 1.5\text{ms}$. When this reflected shock wave hits the gas bubble, a rarefaction wave is reflected which moves towards the elastic wall and the transmitted wave at the water-gas interface is a shock wave that moves through the bubble. Fig. 11(b) shows this effect at the time of 2.0ms . The reflected rarefaction wave from the expanding bubble then hits the elastic wall and gets reflected from the wall, the result of which is the reduction of pressure near the wall. The decrease of pressure continues which culminates in the initiation of cavitation near the wall; the cavitating flow is modeled using the cavitation model developed in [10]. Fig. 11(c) shows the condition at the time of 3.0ms which depicts that cavitation region is growing (the low pressure region as indicated in the figure). This cavitation region

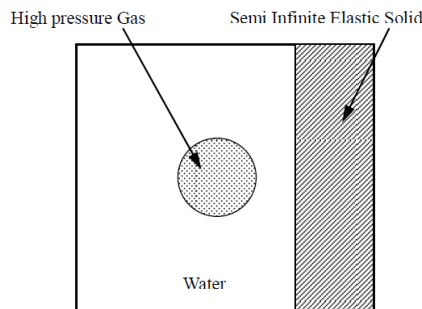


Figure 10: Definition of the problem for Case 4.4.

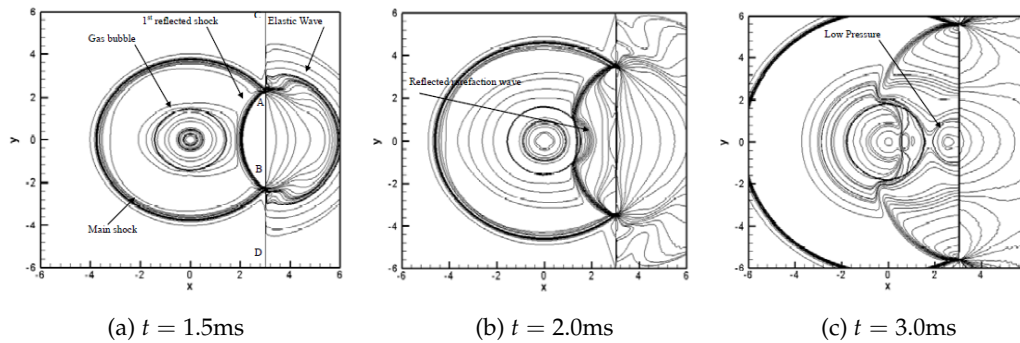


Figure 11: Pressure and $\sigma_{x'x'}$ contour distribution.

then collapses late. At around 3.0ms the main shock moves out of the computational domain. The transmitted shock wave inside the bubble keeps on traveling through the bubble and creates a complex pattern of pressure distribution.

Inside the solid, when the main shock hits the elastic wall, a compressive elastic wave is generated and propagates through it. Fig. 11(a) shows the condition at 1.5ms when the "1st reflected shock wave" is about to hit the gas bubble. The elastic wave moves faster than the shock wave because the acoustic impedance of the elastic solid is much higher than the water (almost more than 2 times in this case). The main shock wave and the 1st reflected shock wave intersect at the solid at two points, where the circular profile of the main shock and 1st reflected shock wave intersects with the water-solid interface. These two "points", *A* and *B* (Fig. 11(a)), move away from the *x*-axis as the shock wave propagate with time. It is these two "points" or regions where large gradient of pressure exists. Beyond these two points up to the boundary (top and bottom), along the interface (*AC* and *BD* in Fig. 11(a)), the compressive elastic wave along the solid surface forms a precursor wave.

5 Conclusions

In this work, the coupling of compressible fluid in the Eulerian coordinate with elastic solid in the Lagrangian system has been studied. The Modified Ghost Fluid Method (MGFM) has been extended and applied to treat the fluid-solid interface, which is tracked using the Level Set technique in the Eulerian coordinate with an extension velocity field obtained using the predicted interfacial velocity. Numerical tests have verified that the present MGFM is capable of providing correct results with robust and consistent performance.

Acknowledgements

This research was partially supported by the National Natural Science Foundation of China (NSFC) (10871018, 10931004) and the National Key Laboratory of Explosion Science and Technology, Beijing Institute of Technology (KFJJ08-7).

References

- [1] D. ADALSTEINSSON AND J. A. SETHIAN, *The fast construction of extension velocities in level set methods*, J. Comput. Phys., 148 (1999), pp. 2–22.
- [2] M. AIVAZIS, W. A. GODDARD, D. MEIRON, M. ORTIZ, J. POOL AND J. SHEPHERD, *A virtual, test facility for simulating the dynamic response of materials*, Comput. Sci. Eng., 2 (2000), pp. 42–53.
- [3] M. ARIENTI, P. HUNG, E. MORANO AND J. SHEPHERD, *A level set approach to Euler-Lagrange coupling*, J. Comput. Phys., 185 (2003), pp. 213–251.
- [4] T. J. CHUNG, *Applied Continuum Mechanics*, Cambridge University Press, 1996.
- [5] R. P. FEDKIW, T. ASLAM, B. MERRIMAN AND S. OSHER, *A non-oscillatory Eulerian approach to interfaces in multimaterial flows (the ghost fluid method)*, J. Comput. Phys., 152 (1999), pp. 457–492.
- [6] R. P. FEDKIW, *Coupling an Eulerian fluid calculation to a Lagrangian solid calculation with the ghost fluid method*, J. Comput. Phys., 175 (2002), pp. 200–224.
- [7] A. FIGUEROA, I. VIGNON-CLEMENTEL, K. JANSEN, T. J. R. HUGHES AND C. A. TAYLOR, *Simulation of blood flow and vessel deformation in three dimensional, patient-specific models of the cardiovascular system using a novel method for fluid-structure interaction*, WIT Transactions on The Built Environment, WIT Press, 84 (2005), pp. 143–152.
- [8] J. J. HEYS, T. A. MANTEUFFEL, S. F. MCCORMICK AND J. W. RUGE, *First-order system least squares (FOSLS) for coupled fluid-elastic problems*, J. Comput. Phys., 195 (2004), pp. 560–575.
- [9] T. G. LIU, B. C. KHOO AND K. S. YEO, *Ghost fluid method for strong shock impacting on material interface*, J. Comput. Phys., 190 (2003), pp. 651–681.
- [10] T. G. LIU, B. C. KHOO AND W. F. XIE, *Isentropic one-fluid modelling of unsteady cavitating flow*, J. Comput. Phys., 201 (2004), pp. 80–108.
- [11] T. G. LIU, B. C. KHOO AND C. W. WANG, *The ghost fluid method for compressible gas-water simulation*, J. Comput. Phys., 204 (2005), pp. 193–221.
- [12] T. G. LIU, B. C. KHOO AND W. F. XIE, *The modified ghost fluid method as applied to extreme fluid-structure interaction in the presence of cavitation*, Commun. Comput. Phys., 1 (2006), pp. 898–919.
- [13] L. G. LIU, W. F. XIE AND B. C. KHOO, *The modified ghost fluid method for coupling of fluid and structure constituted with Hydro-Elasto-Plastic equation of state*, SIAM J. Sci. Comput., 33 (2008), pp. 1105–1130.
- [14] T. G. LIU, J. Y. HO, B. C. KHOO AND A. W. CHOWDHURY, *Numerical simulation of fluid-structure interaction using modified ghost fluid method and Navier equations*, J. Sci. Comput., 36 (2008), pp. 45–68.
- [15] G. H. MILLER AND E. G. PUCKETT, *A high-order Godunov method for multiple condensed phases*, J. Comput. Phys., 128 (1996), pp. 134–164.
- [16] S. OSHER AND J. A. SETHIAN, *Fronts propagating with curvature-dependent speed: algorithms based on Hamilton-Jacobi formulations*, J. Comput. Phys., 79 (1988), pp. 12–49.
- [17] P. PALO, *Survey of naval computational needs in fluid-structure interaction*, IUTAM Symposium on Integrated Modeling of Fully Coupled Fluid Structure Interactions Using Analysis, Computations and Experiments, 1–26, Kluwer Academic Publishers, 2003.
- [18] M. SCHÄFER AND I. TESCHAUER, *Numerical simulation of coupled fluid-solid problems*, Comput. Methods. Appl. Mech. Eng., 190 (2001), pp. 3645–3667.
- [19] M. SCHÄFER, *Coupled fluid-solid problems: surveys on numerical approaches and applications*, PVP-Vol. 460, Emerging Technology in Fluids, Structures and Fluid-Structure Interac-

tions, ASME (2003).

- [20] M. SOULI, K. MAHMADI AND N. AQUELET, *ALE and fluid structure interface*, Mat. Sci. Forum., 465-466 (2004), pp. 143–149.
- [21] H. S. TANG AND F. SOTIROPOULOS, *A second-order Godunov method for wave problems in coupled solid-water-gas systems*, J. Comput. Phys., 151 (1999), pp. 790–815.
- [22] E. F. TORO, *Riemann Solvers and Numerical Methods for Fluid Dynamics: A Practical Introduction*, New York, Springer, 1997.
- [23] H. S. UDAYKUMAR, L. TRAN, D. M. BELK AND K. J. VANDEN, *An Eulerian method for computation of multimaterial impact with ENO shock-capturing and sharp interfaces*, J. Comput. Phys., 186 (2003), pp. 136–177.
- [24] C. W. WANG, T. G. LIU AND B. C. KHOO, *A real-ghost fluid method for the simulation of multi-medium compressible flow*, SIAM Sci. Comput., 28 (2006), pp. 278–302.
- [25] L. XIAO, *Numerical Computation of Stress Waves in Solid*, Akademie Verlag, 1997.
- [26] W. F. XIE, Y. L. YOUNG AND T. G. LIU, *Multiphase modeling of dynamic fluid-structure interaction during close-in explosion*, Int. J. Numer. Methods Eng., 70 (2008), pp. 1019–1043.